Thesis for the Degree of Master of Science

Fabrication and Characterization of Metal (Co, Zn) Oxide Nanofibers by Electrospinning Method

by

Jeong Ha Baek

Department of Chemistry

The Graduate School

Pukyong National University

August 2012

Fabrication and Characterization of Metal (Co, Zn) Oxide Nanofibers by Electrospinning Method
(전기방사 방법을 이용한 금속 (Co, Zn) 산화물 나노섬유의 제조 및 특성)

Advisor Prof. Yong-Cheol Kang

by

Jeong Ha Baek

A thesis submitted in partial fulfillment of the requirements
for the degree of
Master of Science

in Department of Chemistry, The Graduate School,
Pukyong National University

August 2012

Fabrication and Characterization of Metal (Co, Zn) Oxide Nanofibers by Electrospinning Method

A Dissertation

by

Jeong Ha Baek

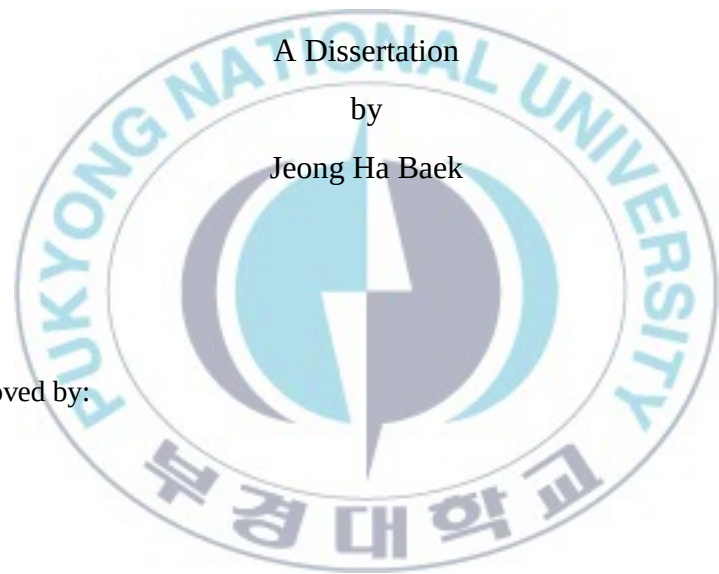

Approved by:

(Chairman) : Don Kim

(Member) : Ju Chang Kim

(Member) : Yong-Cheol Kang

August 25, 2012

CONTENTS

LIST OF FIGURES iii

LIST OF TABLES vi

ABSTRACT vii

CHAPTER 1.Theories 1

1.1. Electrospinning 1

1.2. X-ray Photoelectron Spectroscopy (XPS) 6

1.3. References 14

CHAPTER 2. Spectroscopic and Morphological Investigation of Co_3O_4 Microfibers Produced by Electrospinning Process 15

2.1. Introduction 15

2.2. Experimental Section 18

2.3. Results and Discussion 21

2.3.1. SEM analysis 21

2.3.2. XRD analysis 24

2.3.3. TEM analysis 26

2.3.4. XPS analysis 28

2.4. Conclusion 34

2.5. References 35

CHAPTER 3.Fabrication and Thermal Oxidation of ZnO Nanofibers Prepared via Electrospinning Technique 39

3.1. Introduction 39

3.2. Experimental Section 41

3.3. Results and Discussion 44

3.3.1. SEM analysis 44

3.3.2. XRD analysis 46

3.3.3. TEM analysis 48

3.3.4. XPS analysis 50

3.4. Conclusion 57

3.5. References 58

KOREAN ABSTRACT 62

ACKNOWLEDGMENTS 64

LIST OF FIGURES

Figure 1.1.1.	The nano/micro meter range comparing with the nano/microfiber and human hair.	2
Figure 1.1.2.	Schematic diagram of electrospinning system.	3
Figure 1.1.3.	Detailed schematic diagram of the formation of nanofiber by electrospinning process.	5
Figure 1.2.1.	Schematic diagram of the process of photoionization of core level electron in an atom.	6
Figure 1.2.2.	The components of the XPS instrument and the whole XPS process.	8
Figure 1.2.3.	Schematic diagram of photoelectric effect by X-ray and recoding the data of typical survey spectra of ZnO.	11
Figure 2.1.	SEM images of Co_3O_4 microfibers of (A) Co-rt, (B) Co-873, and (C) Co-1173.	23
Figure 2.2.	XRD pattern for Co microfibers at rt and after calcination at 873 and 1173K. All peaks shown	25

here are cubic Co_3O_4 phase.

Figure 2.3. High resolution TEM images of lattice fringes of the Co_3O_4 microfiber calcined at 1173K and its SAED pattern shown in inset. 27

Figure 2.4. Survey XP spectra of Co-rt, Co-873, and Co-1173. The symbols are represented the Auger peaks; * for Co(LMM), + for Co(LMV), and # for Co(LVV). 29

Figure 2.5. Deconvoluted high resolution (A) C 1s XP spectra (inset is the molecular structure of PVP), (B) Co $2p_{3/2}$ XP spectra, and (C) O 1s XP spectra of Co-rt and Co-1173 microfibers. 30

Figure 3.1. The SEM images of ZnO nanofibers of (a) Zn-rt, (b) Zn-873, and (c) Zn-1173. The size of scale bar in the Figure is 100 nm. 45

Figure 3.2. The XRD patterns of the Zn/PVP nanofibers (Zn-rt) and ZnO nanofibers calcined at different temperatures (Zn-873 and Zn-1173). 47

Figure 3.3. The high resolution TEM images in (a) and (b) and the selected area electron diffraction (SAED) patterns in (c) and (d) of Zn-1173 nanofibers. 49

Figure 3.4. XPS Survey spectra of ZnO nanofibers of Zn-rt, Zn-873, and Zn-1173. 51

Figure 3.5. The deconvoluted high resolution the C 1s XPS spectra of Zn-rt, Zn-873, and Zn-1173. (inset is molecular structure PVP). 53

Figure 3.6. Representative XPS spectra of (a) O 1s and (b) Zn $2p_{3/2}$ of as electospun nanofibers and ZnO nanofibers calcined at 873 and 1173K. 56

LIST OF TABLES

Table 1.2.1.	The XPS notation required for equation (4) by quantum numbers (*n* is principal quantum number).	13
Table 2.1.	The binding energy and atomic ratio of C 1s, O 1s, and Co $2p_{3/2}$ of CoO_x microfibers.	33

Fabrication and Characterization of Metal (Co, Zn) Oxide Nanofibers by Electrospinning Method

Jeong-Ha Baek

Department of Chemistry, Graduate School,

Pukyong National University

Abstract

Materials on the scale of nanometer range have widely been used as research topics because of their interesting characteristics and aspects they bring into the field. In this thesis, the results of fabrication and characterization of micro/nano-fibers of Co and Zn oxides prepared by electrospinning method are reported.

The Co oxide microfibers were synthesized using the electrospinning process and formed Co_3O_4 microfibers after being calcined at high temperatures. The calcination temperature influenced the diameters, morphology, crystalline phase, and chemical environment of the fibers. The surface morphology of the obtained fibers was examined by using the scanning electron microscope (SEM). As the calcination temperatures increased from room temperature to 873 and

1173K, the diameters of the cobalt oxide fibers decreased from 1.79 to 0.82 and 0.32 μm, respectively. The structure of the fibers was investigated with X-ray diffraction (XRD) and transmission electron microscopy (TEM). The calcined Co_3O_4 fibers had crystalline face-centered cubic (fcc) structure. The X-ray photoelectron spectroscopy (XPS) results revealed that increasing the calcination temperature promoted the formation of Co^{2+} and Co^{3+} species.

Out of the many metal oxides, zinc oxide (ZnO) was chosen to be fabricated as nanofibers using the electrospinning method for potential uses of solar cells and sensors. After ZnO nanofibers were obtained, calcination temperature effects on the ZnO nanofibers were studied and report here. The results of SEM revealed that the aggregation of the ZnO nanofiber was progressed by calcination. XRD study showed the hcp ZnO structure was enhanced by calcination at 873 and 1173K. TEM confirmed the crystallinity of the calcined ZnO nanofibers. XPS verified the thermal oxidation of Zn species by calcination in the nanofibers. These techniques have helped us deduce the facts that the diameter of ZnO increases as the calcination temperature was raised; the process of calcination affects the crystallinity of ZnO nanofibers, and the thermal oxidation of Zn species was observed as the calcination temperature was raised.

CHAPTER 1. Theories

1.1. Electrospinning

‘Electrospinning process’ offers a good top-down method for production of nano/micro sized materials and simple process for composing high surface area. Moreover, the obtained nano/microfibers using electrospinning method have been composed with the precursor of pure polymer and various inorganic oxide species. So, a variety of metal oxides are produced by electrospinning method containing binary, ternary, and quaternary. Those products have chemical and physical properties for adopting broad range of applications such as solar cells, rechargeable batteries, electronic devices, super-capacitors, and gas sensors [1-3]. The brief theory about nanofibers, electrospinning system, and its parameters will be discussed.

The nanofibers are defined in the range from 10 to 1000 nm in diameter as shown in Figure 1.1.1. They have prominent characteristics. As it is well known, the physical and chemical properties of materials are affected by their size and shape. The nano/microfibers are thinner and finer than normal fibers in size. The surface to volume ratio of nano/microfibers is increased and the pore diameter is decreased. The diameter of fabricated nano/microfibers using electrospinning method can be controlled by spinning parameters.

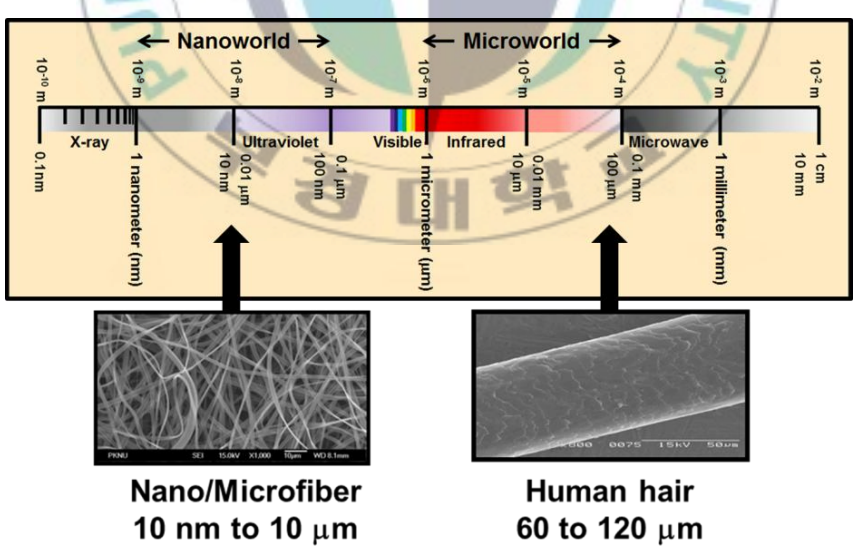

Figure 1.1.1. The nano/micro meter range comparing with the nano/microfiber and human hair.

The parameters for running the electrospinning are below;

1. Organic/inorganic solution,
2. Viscosity, conductivity, surface tension, electric potential (high voltage), feed rate, and distance between the tip and the collector,
3. Concentration of solution, temperature, and humidity,
4. Speed of revolution of the collector and the diameter of needle.

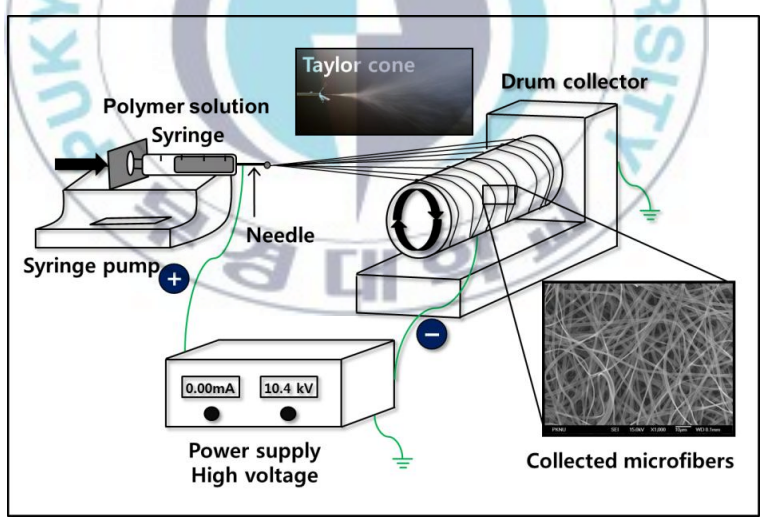

Figure 1.1.2. Schematic diagram of electrospinning system.

Figure 1.1.2 is the whole schematic diagram of electrospinning system. The electrospinning apparatus is composed with syringe part, high voltage power supply, and a drum collector. Syringe part is composed with a needle, syringe pump, and precursor solution in the syringe. The syringe pump maintains constant feed rate, so the precursor solution is jetted and form a droplet as shown in Figure 1.1.3. When high voltage using power supply is applied between the syringe needle and the drum collector, a droplet expands and forms Taylor cone [4]. At this point, if the surface charge of the droplet has to offset the surface tension of the droplet, Taylor cone and microfiber will acquire on the drum collector. The drum collector must spin constant rate to get constant form of microfibers. The electrospinning technique provides a method for synthesis of micro/nano-fibers relatively easily, and also takes short amount time for the synthesis [5].

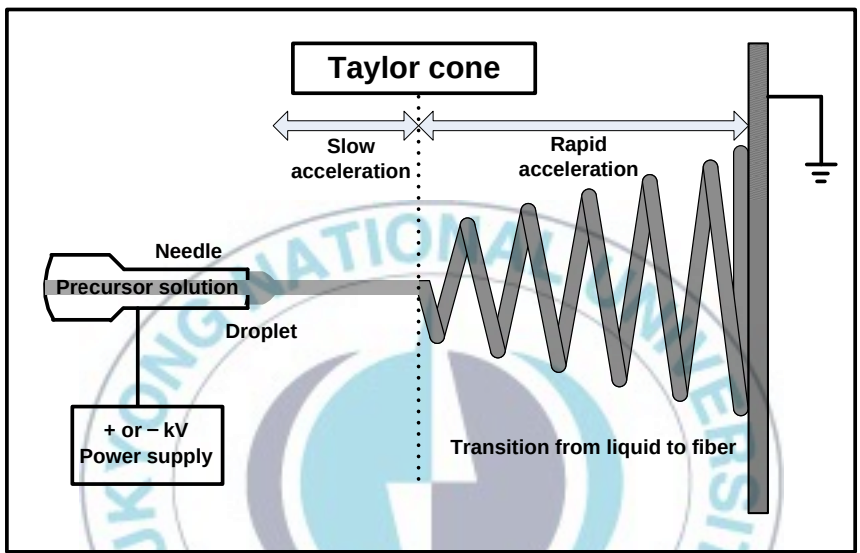

Figure 1.1.3. Detailed schematic diagram of the formation of nanofiber by electrospinning process.

1.2. X-ray Photoelectron Spectroscopy (XPS)

X-ray photoelectron spectroscopy (XPS) is a quantitative and spectroscopic technique which makes possible to analyze the elemental composition, empirical formula, electronic state, and chemical nature of the elements in the surface region of sample by recording the unique binding energy of core electrons. XPS is also known as ESCA (Electron Spectroscopy for Chemical Analysis) for surface sensitive chemical analysis technique. XPS must need ultra-high vacuum (UHV, $P<10^{-9}$ Torr) condition because of the weak signal from the surface region of sample.

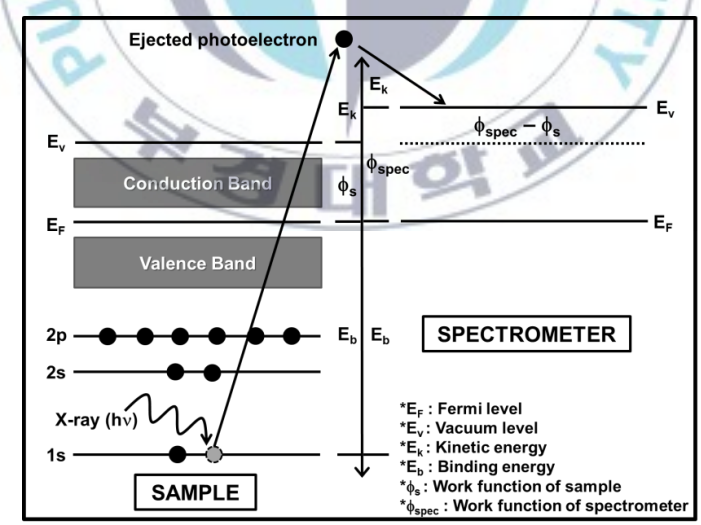

Figure 1.2.1. Schematic diagram of the process of photoionization of core level electron in an atom.

The schematic diagram of the XPS process is shown in Figure 1.2.1. The binding energy of filled core electrons located at closing an atomic nucleus corresponds to X-ray region. When the core electron absorbs the X-ray ($h\nu$), which is larger than the binding energy (E_b) of core electron, a photoelectron is emitted over vacuum level (E_v) from the atom. The energy of the electron have 'chemical shift' dependent on the oxidation state and chemical environment of the atom which can be verified by peak deconvolution process. In order to understand the chemical shift of core electron in binding energy, the process of photoionization and the energy relationship of E_k, E_b, and ϕ should be considered by representing a formula as follow:

$$A + h\nu \rightarrow A^{+} + e^{-} \qquad (1)$$

And then conservation of the energy requires that:

$$E_k = h\nu - (E_b + \phi_{spec}) \qquad (2)$$

where, E_k is the kinetic energy of photoelectron, h is plank's constant (6.62×10^{-34} [Js]), ν is the frequency [Hz] of X-ray, E_b is the binding energy of the electron, and ϕ_{spec} is the work function of

the spectrometer. If the (E_b+ ϕ_{spec}) is represented as *BE*, and E_k is called as *KE*, the formula (2) can be represented following simple equation (3).

$$KE = h\nu - BE \qquad (3)$$

Because the energy of X-ray ($h\nu$) with particular wavelength and the kinetic energy of photoelectron are known, the binding energy (*BE*) of ejected electron can be deduced by using the equation (3) that is based on the work of Ernest Rutherford [5-6]. In Figure 1.2.2, the essential components of the XPS instrument and XPS process are shown.

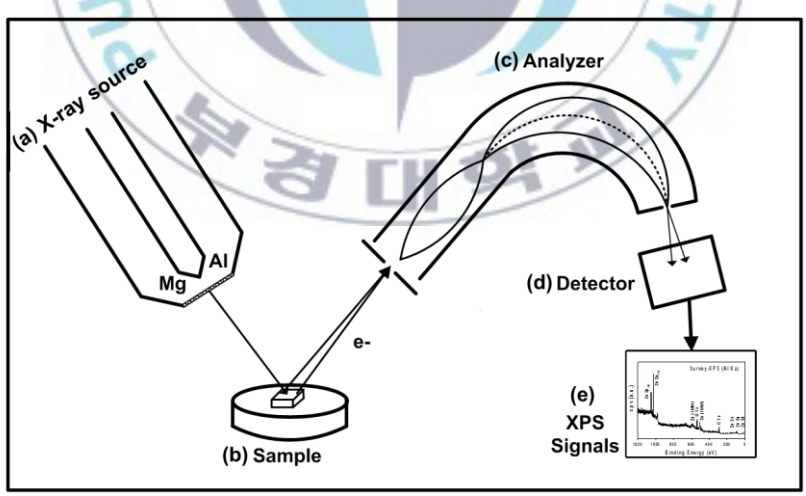

Figure 1.2.2. The components of the XPS instrument and the whole XPS process.

The components of XPS system are

(a) X-rays source ($h\nu$)

· Mg Kα radiation: 1253.6 eV

· Al Kα radiation: 1486.6 eV

(b) Sample

· UHV compatibility: low vapor pressure

· Thin films, ceramic, superconductor, oxide powder, polymer, etc.

(c) Analyzer

· CHA (Concentric Hemispherical Analyzer)

· Electronic focusing lens system

(d) Detector

· SEM (Secondary Electron Multiplier)

· Channeltron

(e) Data acquisition system.

The analyzer allows a selection in energy of the ejected electrons. These selected photoelectrons will arrive at the detector which makes it possible to analyze secondary electron. Eventually, the XPS signal could be collected due to the experimentally determined *BE* of elements which are characteristic of specific element. More detail explanation of the acquisition of XPS spectrum is shown in Figure 1.2.3 schematically. The XPS gives information about the existence of the specific element. Moreover, the intensity of peak in spectra is related to the concentration of specific element. A survey spectrum of the emitted photoelectrons in ZnO sample using Al Kα radiation is shown in the inset of Figure 1.2.3.

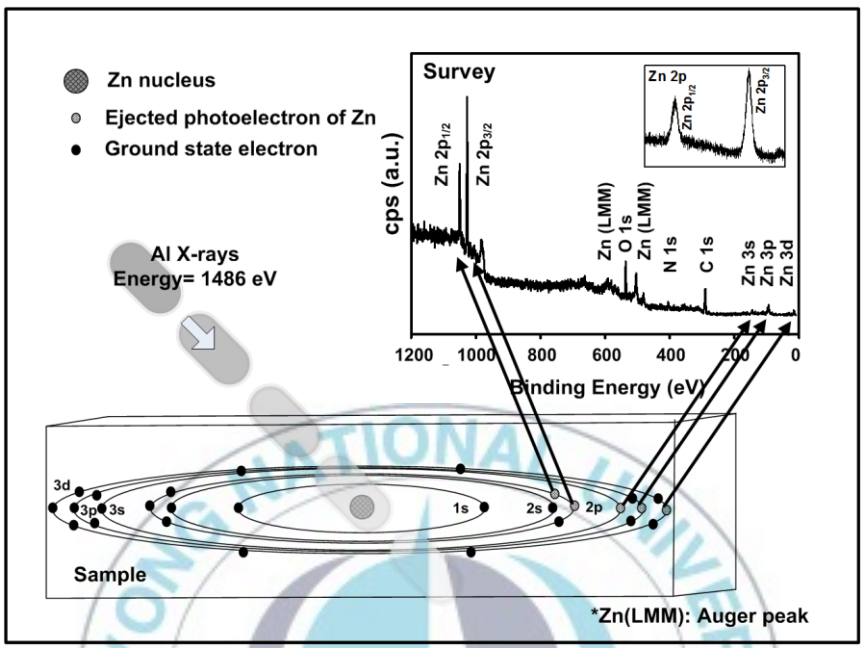

Figure 1.2.3. Schematic diagram of photoelectric effect by X-ray and recoding the data of typical survey spectra of ZnO.

The survey spectrum has actual peak of particular element from emitted electron. Auger peaks and satellite features, which supply secondary information of sample, are observed as well. The Zn 2p photoemission line is split to doublets those named as Zn $2p_{1/2}$ and Zn $2p_{3/2}$ with an intensity ratio of 1:2. Which is called as SOS (Spin-Orbital Splitting).This separation is observed from p, d, and f electrons. Removal of core electrons of the elements in ZnO by

X-ray leads to ionization, and then LS coupling occurs. If we consider the Zn 2p sub-shell, the peak notation with total angular momentum quantum number (j) and peak intensity ratio can be measured as follow equation (4):

$$j = l + s \qquad (l = 1,\ s = \pm 1/2) \qquad (4)$$

	Notation		Ratio
$j_1 = 1 + 1/2 = 3/2$	$\rightarrow$ $Zn\ 2p_{3/2}$	$\rightarrow\ 2\times\{3/2\}+1 = 4$	$\rightarrow$ 2
$j_2 = 1 - 1/2 = 1/2$	$\rightarrow$ $Zn\ 2p_{1/2}$	$\rightarrow\ 2\times\{1/2\}+1 = 2$	$\rightarrow$ 1

where, l is orbital angular momentum quantum number and s is spin angular momentum quantum number. The XPS notation is shown in table 1.2.1.

Table 1.2.1. The XPS notation required for equation (4) by quantum numbers (*n* is principal quantum number).

Orbital	Quantum Numbers				Notation
	n	*l*	*s*	*j*	
s	1	0	±1/2	1/2	$1s_{1/2}$
p	2	0	±1/2	1/2	$2s_{1/2}$
	2	1	–1/2	1/2	$2p_{1/2}$
	2	1	+1/2	3/2	$2p_{3/2}$
d	3	0	±1/2	1/2	$3s_{1/2}$
	3	1	–1/2	1/2	$3p_{1/2}$
	3	1	+1/2	3/2	$3p_{3/2}$
	3	2	–1/2	3/2	$3d_{3/2}$
	3	2	+1/2	5/2	$3d_{5/2}$
f	4	0	±1/2	1/2	$4s_{1/2}$
.	.	.	.	.	.

1.3. References

[1] Guo, J.; Song, Y.; Chen, D.; Jiao, X. *J. Dis. Sci. Tech.* **2010**, *31*, 684.

[2] Sangkhaprom, N.; Supaphol, P.; Pavarajarn, V. *Ceram. Intern.* **2010**, *36*, 357.

[3] Yun, S.; Lim, S. *J. Collo. Interf.* **2011**. *360*, 430.

[4] Taylor, S. G. *Proc. Roy. Soc.***1964**, *280*, 392.

[5] Turner, D. W.; Jobory, M. I. *J. Chem. Phys.***1962**, *37*, 3007.

[6] Sieghahn, K. *Rev. Mod. Phys*. **1982**, *54*, 709.

CHAPTER 2.

Spectroscopic and Morphological Investigation of Co_3O_4 Microfibers Produced by Electrospinning Process

2.1. Introduction

Nano-/micro-structured transition metal oxide materials have been actively studied because of their scientific interests and various usages in applications including catalysts, electronics, photonics, and sensors [1-5]. Compare to bulk metal oxide materials, the nano-/micro-scaled metal oxide materials have large surface to volume ratio and a high level of crystallinity. These can affect chemical, physical, and electrical properties.

There are three well known polymorphs of cobalt oxides, and they are cobaltous oxide (CoO), cobaltic oxide (Co_2O_3), and cobaltosic oxide (Co_3O_4). These cobalt oxides are interesting due to their useful chemical and physical properties [6]. Co_3O_4 is

especially more attractive than the other Co oxides, because of its potential applications such as magnetic materials in energy storages [7], sensors [8], and heterogeneous catalysts [9,10]. Moreover, Co_3O_4 is used in supercapacitors [11,12], lithium ion batteries [13,14], electrochromic devices [15], reduction [16], and oxygen evolution [17] as electrode materials.

Microsized Co_3O_4 can be synthesized by different methods such as spray pyrolysis [7], hydrothermal [14], wet chemicals [18], sputtering [19], thermal decomposition [17], electrochemical deposition [11,20], sol-gel [21], microwave assisted deposition [22], electrospinning [23-25], and chemical vapor deposition [26]. Among them, the electrospinning process provides a simple and facile method for synthesizing fibers, which are one of the one-dimensional structural materials. Those microfibers are incorporated with polymer/inorganic composites as a precursor in the range of micrometers. Moreover, not only the electrospinning technique can easily synthesize microfibers of controlled sizes and shapes, but also takes a relatively short amount of time to synthesize. Overall, we synthesized Co_3O_4

microfibers by using the electrospinning process.

Recently, some studies have succeeded in synthesizing cobalt oxide nanofibers by using the electrospinning method [6,27]. However, reports about the effect of calcination temperature on the chemical and physical properties of the Co_3O_4 microfibers are sparse. We report that the calcination temperature effect on the electrospun Co_3O_4 microfibers which were characterized with scanning electron microscopy (SEM), X-ray diffraction (XRD), transmission electron microscopy (TEM), and X-ray photoelectron spectroscopy (XPS).

2.2. Experimental Section

Cobalt oxide microfibers were produced by electrospinning technique using cobalt nitrate ($Co(NO_3)_2 \cdot 6H_2O$, MW: 291.03, Junsei Chemical) and polyvinylpyrrolidone (PVP, $(C_6H_9NO)_x$, MW:~1,300,000, Sigma Aldrich) solution. The cobalt nitrate solution was made with 0.6 g of cobalt nitrate in 13 ml of ethanol (99.9 %) and it was stirred for 1 hr at room temperature. Then 0.77 g of PVP was added in the cobalt nitrate solutions and was stirred for 11 hrs to stabilize at rt. The mixed solution was used for a precursor solution. The viscosity of the precursor solution was measured with a viscometer (A&D; SU-10) and the average viscosity was 85.03 (± 3.31) cP. It is important to control the viscosity of the solution for obtaining microfibers because viscosity is a crucial factor for the formation of microfibers without beads.

The precursor solution in a syringe (10 ml) was pumped by a syringe pump (KDS scientific) and was electrospun to a drum collector, which was covered with aluminum foil. The distance

between the tip and the collector was kept constant at 15 cm and the speed of the revolution of the drum was maintained at 100 rpm during the electrospinning process. The applied average voltage between the collector and the syringe tip was 12.1 kV. The obtained cobalt oxide (CoO_x) microfiber composites were heated in a tube furnace (DTF-40300-12T, Daeheung Scientific Co.) for 5 hrs at 353K for evaporation of residual ethanol used as a solvent. The solvent-free microfibers were calcined at 873 and 1173K in a tube furnace in order to obtain cobalt oxide microfibers. The obtained cobalt oxide (CoO_x) microfibers are called Co-873 and Co-1173 hereafter. Those temperatures were chosen based on the result of thermogravimetric analysis [28].

Surface morphology of the CoO_x nanofibers was observed by means of field-emission scanning electron microscopy (FE-SEM, JEOL, JSM-6700F). Transmission electron microscopy (TEM, JEOL, JEM-2010) images of the CoO_x microfibers were taken to check the lattice parameters. X-ray diffraction (XRD, PHILIPS, X'Pert-MPD System) patterns were recorded for identification of the phase of the CoO_x microfibers. The chemical

nature of the CoO_x microfibers was studied with X-ray photoelectron spectroscopy (XPS, VG ESCALAB 2000) using Mg Kα X-ray source (1253.6 eV). The base pressure in the analysis chamber was kept lower than 8.2×10^{10} Torr.

2.3. Results and Discussion

2.3.1. SEM analysis

The morphology of obtained CoO_x microfiber was investigated with SEM. The SEM images of the as-electrospun (Co-rt) and calcined CoO_x microfibers are shown in Figure 2.1. The average diameters of Co-rt, Co-873, and Co-1173 were 1.79 (± 0.20), 0.82 (± 0.19), and 0.32 (± 0.10) μm, respectively. The diameter, comparing Co-rt with those of Co-873 and Co-1173, reduced to 54.73% and 81.62%, respectively. As the calcination temperature increased, the diameter of microfibers drastically decreased. The surface of Co-rt was smooth and continuous. After calcination at 873K, the surface of microfibers turned coarse shown in Figure 2.1 (B) and some submicro-tunnels were formed. This implies that the PVP in Co-rt microfibers was decomposed by calcination at 873K [29]. A similar phenomenon in morphology change of nanowires was reported by Z. Hou *et al.* [30]. As shown in Figure 2.1 (C), the CoO_x microfibers seemed to be connected with submicro-sized CoO_x particles, eventually the 1D microfiber

vanished and a 3D network formed. The conceptual process of 3D network of CoO_x formation is depicted under the SEM images. It may be due to the removal of PVP during the calcination process and aggregated the submicro-sized particles and pores formed. Those observations suggest that the PVP in the microfibers acted as a framework of the PVP/$Co(NO_3)_2$ composite microfibers before calcination and CoO_x microfibers formed after calcination. Therefore the calcination temperature influenced the shape and diameter of CoO_x microfibers.

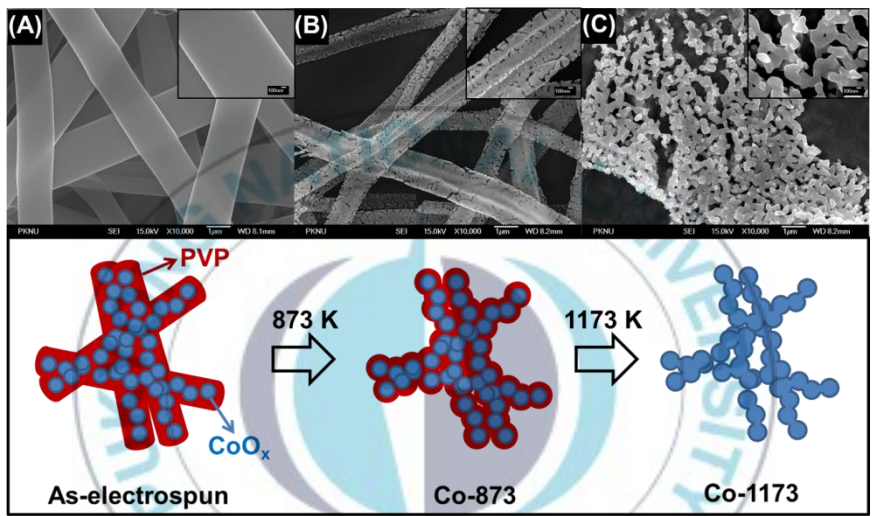

Figure 2.1. SEM images of Co_3O_4 microfibers of (A) Co-rt, (B) Co-873, and (C) Co-1173.

2.3.2. XRD analysis

XRD analysis was performed to investigate the phase of the CoO_x microfibers. Figure 2.2 shows the XRD patterns of Co-rt and calcined CoO_x microfibers. No characteristic peaks, corresponding to metallic Co or Co oxide were detected from Co-rt microfibers except the broad band at $2\theta = 24.57^o$, which is attributed to the semi-crystalline PVP [24]. It indicates that the amorphous phase was dominant before calcination. After calcination at 873 and 1173K, well defined diffraction peaks evolved. This result revealed that the PVP in the CoO_x microfibers decomposed and the crystallinity of CoO_x microfibers established due to the formation of fcc-Co_3O_4 phase [31]. The crystal size of the Co_3O_4 was calculated by Scherrer's equation [32] using the Co_3O_4 (311) peak. The crystal size in the Co-873 microfibers was about 46.71 (± 0.04) nm and increased to 53.21 (± 0.17) nm for Co-1173. The increase of the crystal size could be caused by aggregating nanoparticles in the CoO_x microfibers during calcination.

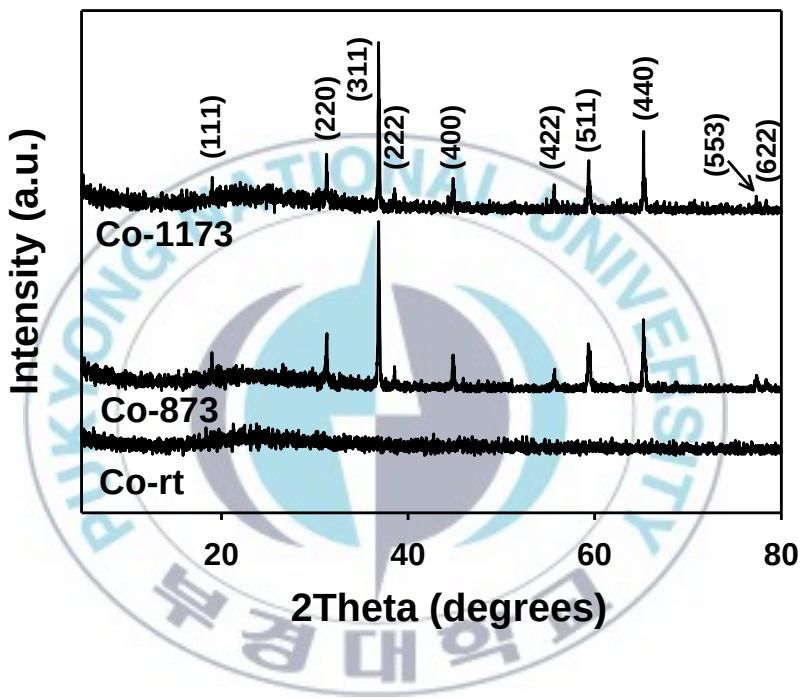

Figure 2.2. XRD pattern for Co microfibers at rt and after calcination at 873 and 1173K. All peaks shown here are cubic Co_3O_4 phase.

.

2.3.3. TEM analysis

To verify the crystallinity of the Co_3O_4 microfibers TEM images were collected. The representative TEM image of Co-1173 is shown in Figure 2.3. The high resolution TEM image shows the uniform arrangement of the lattice plane approving the crystallinity with 0.45 (± 0.06) nm of interplane spacing corresponding to the (111) plane of the Co_3O_4 [28]. The imperfectness of the crystal hardly detected in the lattice fringes which implies the Co-1173 contains good crystallinity. The lattice fringes of the selected area electron diffraction (SAED) image are depicted in the inset of Figure 2.3. Indices of the SAED pattern correspond to $(1\bar{1}1)$, $(\bar{1}1\bar{1})$, (420), and $(33\bar{1})$ planes from crystallographic simulations [33]. This indicates that the crystalline Co_3O_4 formed after calcination at high temperature.

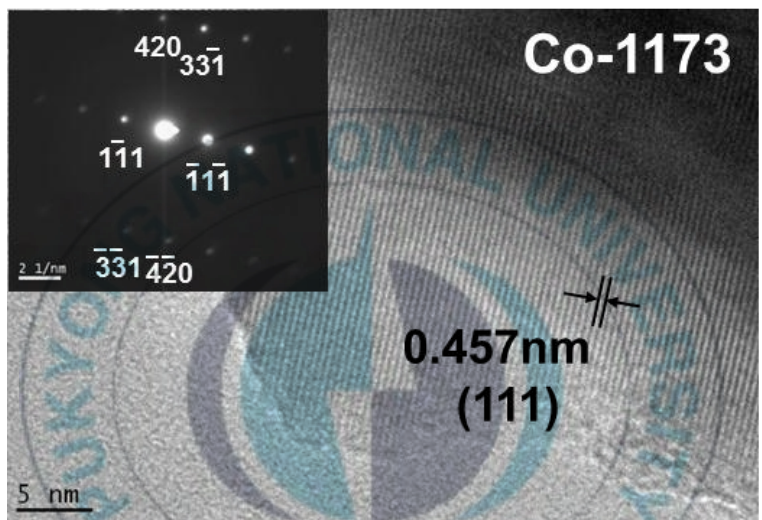

Figure 2.3. High resolution TEM images of lattice fringes of the Co_3O_4 microfiber calcined at 1173K and its SAED pattern shown in inset.

2.3.4. XPS analysis

XPS was performed for investigation of the chemical nature of CoO_x microfibers. Figure 2.4 shows the survey XP spectra of Co microfibers. Characteristic peaks of Co, O, N, and C and the Auger lines of Co(LMM), Co(LMV), and Co(LVV) evolved at different calcinations temperatures. The N 1s peak was observed at Co-rt, but it vanished as the calcination temperature increased. The calcination process caused the decomposition of PVP and removal of nitrogen. The intensity of C 1s peak decreased, however the Co 2p and O 1s peaks increased as the calcinations temperature increased.

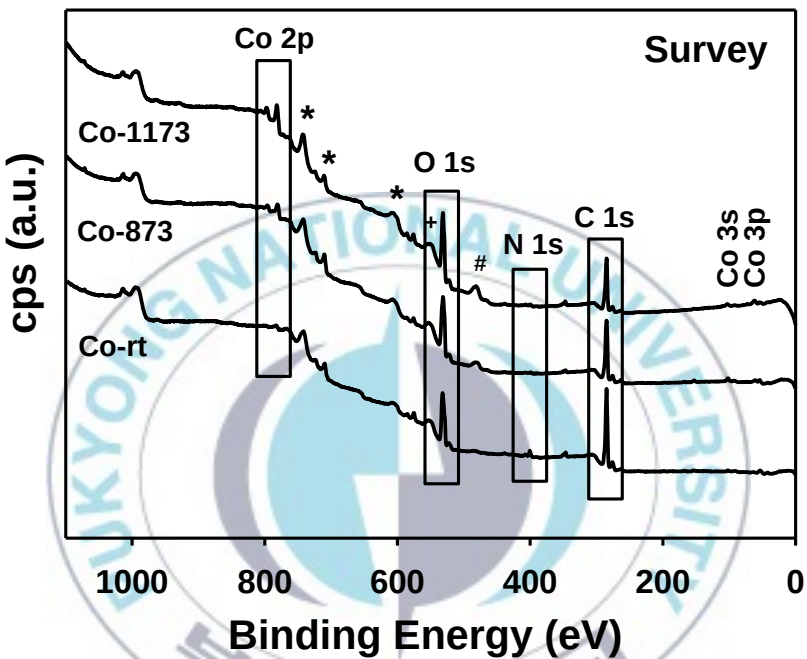

Figure 2.4. Survey XP spectra of Co-rt, Co-873, and Co-1173. The symbols are represented the Auger peaks; * for Co(LMM), + for Co(LMV), and # for Co(LVV).

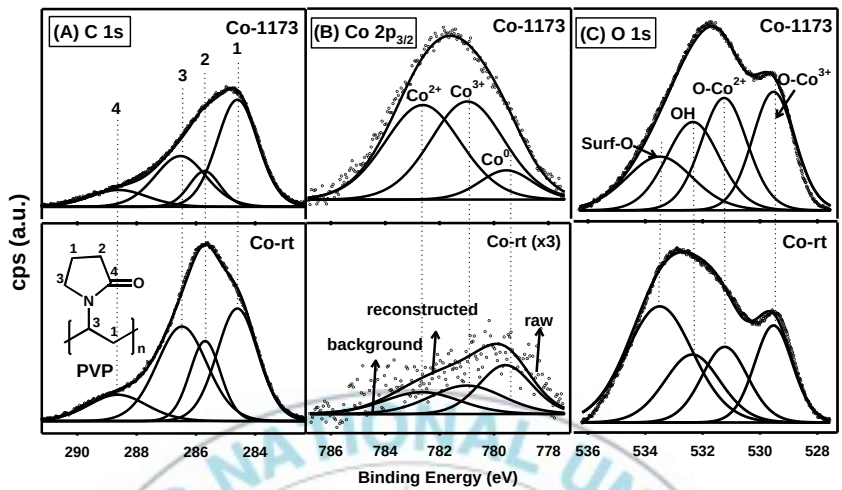

Figure 2.5. Deconvoluted high resolution (A) C 1s XP spectra (inset is the molecular structure of PVP), (B) Co $2p_{3/2}$ XP spectra, and (C) O 1s XP spectra of Co-rt and Co-1173 microfibers.

The Figure 2.5 shows the representative deconvoluted high resolution XP spectra of C 1s, Co 2p, and O 1s. The C 1s peak decomposed to 4 peaks which are attributed to the carbon with different chemical environments in PVP [34]. The detailed parameters are listed in Table 1. The numbers for carbon denoted in Figure 2.5 (A) are assigned from low to high binding energy depending on its chemical environment. The relative ratio of 1, 2, 3, and 4 is almost 2:1:2:1 for Co-rt. The intensities of 3(C-N) and

4(C=O) decreased with increasing calcination temperatures. Due to the closed calcination system for the microfibers, the decomposed PVP might redeposit on the surface of microfibers during the calcination process. Therefore the components of residual PVP were detected after calcination. These results demonstrate the decomposition of PVP and support the results of SEM observation. The oxidation state of cobalt can be deduced from the deconvoluted XP spectra of O 1s and Co 2p. Figure 2.5 (B) shows the deconvoluted XP spectra of Co $2p_{3/2}$ of CoO_x microfibers obtained at different calcination temperatures. The Co $2p_{3/2}$ region was deconvoluted to avoid complexity because the spin obit splitting constant of Co is large, which is 15.1 eV. The deconvoluted Co $2p_{3/2}$ peaks were assigned to Co^0, Co^{3+}, and Co^{2+} from low to high binding energy [35-37]. The binding energy of the Co^{3+} with tetrahedral geometry (high spin) was assigned to lower than that of Co^{2+} with octahedral structure (low spin). [38] Information about the binding energy and relative ratio of each species with different oxidation state is listed in Table 2.1. As the calcinations temperature increased to 1173K, the Co intensity

increased due to the decomposition of PVP which caused exposure of Co species on the surface region of microfibers. The relative ratios of Co^{2+} and Co^{3+} increased whereas Co^{0} decreased. It is worthy to note the ratios of Co species comparing in Co-873 and Co-1173. As the calcination temperature increased, Co^{3+} ratio was almost constant, however that of Co^{2+} increased and Co^{0} decreased. This result reveals that the thermal energy promotes oxidation of Co^{0} to higher oxidation states during calcination at 1173K. This energy could be enough to oxidize Co^{0} to Co^{2+} but it was insufficient to oxidize to Co^{3+}. The relative ratio of O-Co^{2+} and O-Co^{3+} peaks in O 1s XP spectra shows similar to Co XPS result. The O 1s spectra were deconvoluted to four contributions as shown in Figure 2.5 (C). The first contribution was O-Co^{3+} and second was O-Co^{2+}. Intensities of these peaks increased with an increase of calcination temperature. It is interesting to compare the relative ratios of O-Co^{2+} and O-Co^{3+}. The relative ratio of oxygen species bound with Co^{2+} increased more comparing with that of O-Co^{3+}. This result supports the Co XPS result that the oxidation of Co was promoted by thermal energy. The third peak was assigned to the

oxygen in the form of hydroxyl group, and fourth peak corresponded to the oxygen near surface region of the microfibers. As the calcination temperature increased, the contents of surface oxygen decreased

Table 2.1. The binding energy and atomic ratio of C 1s, O 1s, and Co $2p_{3/2}$ of CoO_x microfibers.

	Peak assignment	Co-rt		Co-873		Co-1173	
		BE (eV)	Ratio (%)	BE (eV)	Ratio (%)	BE (eV)	Ratio (%)
C 1s	C-C (1)	284.6	34.6	284.6	42.3	284.6	48.6
	C-C=O (2)	285.7	18.5	285.7	13.9	285.7	12.1
	C-N (3)	286.5	35.5	286.5	32.9	286.5	28.5
	C=O (4)	288.6	11.5	288.6	10.9	288.6	10.7
Co $2p_{3/2}$	Co^0	779.5	40.8	779.5	21.8	779.5	9.7
	Co^{3+}	781.0	33.0	781.0	45.2	781.0	45.3
	Co^{2+}	782.7	26.2	782.7	33.0	782.7	45.0
O 1s	O-Co^{3+}	529.5	19.7	529.5	27.1	529.5	27.2
	O-Co^{2+}	531.2	18.6	531.2	24.0	531.2	27.1
	OH	532.3	20.3	532.3	20.6	532.3	25.4
	Surf-O	533.5	41.4	533.5	28.3	533.5	26.5

2.4. Conclusion

The Co oxide microfibers were produced with cobalt nitrate ($Co(NO_3)_2$)/polyvinylpyrollidone (PVP) precursor solutions by using the electrospinning technique. As a result, Co_3O_4 fibers were formed after calcination at 873 and 1173K. The SEM images reveal that the diameter of electrospun microfibers decreased as the calcination temperature increased. The XRD results show that electrospun CoO_x formed as an amorphous phase and the crystalline Co_3O_4 phase (fcc) formed after calcinations at high temperature. The crystal size of Co_3O_4 in the microfibers increased as the calcination temperature increased. The TEM images verified the crystallinity of Co_3O_4 microfibers correspond to the (111) plane. The XPS results reveal that the PVP in CoO_x microfibers decomposed and Co^0 species was oxidized to Co^{2+} species by thermal energy due to an increase in calcination temperature. But Co^0 did not oxidize to Co^{3+} because the thermal energy at 1173K might not have been high enough. Therefore, the calcination temperature affected the morphology, diameter, and oxidation state of the CoO_x microfibers.

2.5. References

[1] Hu, J.Q.; Ma, X. L.; Shang, N. G. *J. Phys. Chem. B.* **2002**, *106*, 3823.

[2] Xia, Y.; Yang, P.; Sun, Y. *Adv. Mater.* **2003**, *15*, 353.

[3] Luo, S.; Fan, J.; Liu, W. *Nanotechnology.* **2006**, *17*, 1695.

[4] Chaudhari, G. N.; Bambole, D. R.; Bodade, A. B. *J. Mater. Sci.* **2006**, *41*, 4860.

[5] Chen, C. L.; Weng, H. S. *Appl. Catal. B.* **2005**, *55*, 115.

[6] Yu, D.; Ying, W.; Liang, S.; Michael, B.; Heng Z.; Yu, L. *Biosen. Bioelec.* **2010**, *26*, 542.

[7] Noguchi, S.; Mizuhashi, M. *Thin Solid Films.* **1981**, *77*, 99.

[8] Logothesis, E. M.; Park, K.; Meitzler, A. H.; Laud, K. R. *Appl. Phys. Lett.* **1975**, *26*, 209.

Chun, M. S.; Moon, M. J.; Park, J.; Kang, Y. C. *Bull. Korean Chem. Soc.* **2009**, *30*, 2729.

[9] Szegedi, A.; Popova, M.; Mavrodinova, V.; Minchev, C. *Appl. Catal. A.* **2008**, *338*, 44.

[10] Kim, H.; Park, D. W.; Woo, H. C.; Chung, J. S. *Appl. Catal. B.* **1998**, *19*, 233.

[11] Hu, C. C.; Cheng, C. Y. *Electrochem. Solid-State Lett.* **2002**, *5*, A43.

[12] Hosono, E.; Fujihara, S.; Honma, I.; Ichihara, M.; Zhou, H. *J. Power Sources.* **2006**, *158*, 779 .

[13] Wang, H.; Jang, Y.I.; Huang, B.; Sadoway, D. R.; Chiang, Y. M. *J. Electrochem. Soc.* **1999**, *146*, 473.

[14] Liu, Y.; Mi, C.; Su, L.; Zhang, X. *Electrochim. Acta.* **2008**, *53*, 2507.

[15] Monk, P. M. S.; Ayub, *S. Solid State Ionics.* **1997**, *99*, 115.

[16] Schumacher, L. C.; Holzhueter, I.; Hill, I. R.; Dignam, M. *J. Electrochim. Acta.* **1990**, *35*, 975.

[17] Hu, C. C.; Chen, C. A. *J. Chin. Inst. Chem. Eng.* **1999**, *30*, 431.

[18] Casella, I. G.; Gatta, M. *J. Electroanal. Chem.* **2002**, *534*, 31.

[19] Salah A.; Makhlouf *J. Magn. Magn. Mater.* **2002**, *246*, 184.

[20] Schumacher, L. C.; Hill, I. R.; Dignam, M. *J. Electrochim. Acta.* **1990**, *35*, 975.

[21] Spinolo, G.; Ardizzone, S.; Trasatti, S. *J. Electroanal. Chem.* **1997**, *423*, 49.

[22] Casella.; Innocenzo, G. *J. Electroanal. Chem.* **2002**, *520*, 119.

[23] Shao, C. L.; Kim, H. Y.; Gong, J.; Lee, D. R. *Nanotechnology* **2002**, *13(5)*, 635.

[24] Ramaseshan, R.; Sundarrajan, S.; Jose, R.; Ramakrishna, S. *J. Appl. Phys.* **2007**, *102*, 111101.

[25] Dan, Li.; Younan, X. *Adv. Mater*. **2004**, *16*, 1151.

[26] Yu, Z. G.; Yang, B. C. *Mater. Lett.* **2008**, *62*, 211.

[27] Hongyu, G.; Changlu, S.; Shangbin, W.; Bin, C.; Jian, G.; Xinghua, Y. *Mater. Chem. Phys.* **2003**, *82*, 1002.

[28] Jo, J. M.; Park, J.; Kim, D.; Koh, S. W.; Kang, Y. C. *Bull. Korean Chem. Soc.* **2010**, *31*, 1776.

[29] Hwang, A. R.; Park, J.; Kang, Y. C. *Bull. Korean Chem. Soc.* **2011**, *32*, 3338.

[30] Zhiyao, H.; Chunxia, L.; Jun, Y.; Hongzhou, L.; Piaoping, Y.; Ruitao, C.; Ziyong, C.; Jun, L. *J. Mater. Chem*. **2009**, *19*, 2737.

[31] JCPDS Database, International Center for Diffraction Data **1997**, PDF 73-1969.

[32] Klong, H. P.; Alexander, L. E. X-*ray Diffraction Procedures for Crystalline and Amorphous Materials*, Wiley: New York, **1954**;

pp 491-538.

[33] Wang, Y.; Zhong, Z.; Chen, Y.; Ng, C.T.; Lin, J. *Nano Res*. **2011**, *4*, 695.

[34] Jiang, P.; Zhou, J. J.; Li, R.; Wang, Z. L.; Xie, S. S. *Ins. Phy. Pub. Nano.* **2006**, *17*, 3533.

[35] Xu, X. L.; Chen, Z. H.; Li, Y.; Chen, W. K.; Li, J. Q. *Sur. Sci.* **2009**, *603*, 653.

[36] Helena, A. E.; Hagelin-W.; Gar, B. H.; David, M. M.; Ghaleb, N. S. *Appl. Surf. Sci.* **2004**, *235*, 420.

[37] Petitto, S. C.; Langell, M. A. *J. Vac. Sci. Technol*. **2004**, *A22*, 4.

[38] Altavilla, A.; Ciliverto, E. *Appl. Phys. A.* **2004**, *79*, 309.

CHAPTER 3.
Fabrication and Thermal Oxidation of ZnO Nanofibers Prepared via Electrospinning Technique

3.1. Introduction

One-dimensional (1D) nano-materials with high surface to volume ratio have attracted attention because of their exceptional chemical and physical properties and various applications [1-3]. There are many kinds of 1D nanostructures such as nano-belts[4], nanoneedles [5], nanorods [6], nanorings [7], nanowires [8], nanotubes [9], and nanofibers [10]. These materials can be produced using various methods such as the sol-gel process [11], sputtering [12], spray pyrolysis [13], hydrothermal [14], electrospinning [15-16], and electrochemical deposition [17]. Among these techniques pertaining to the 1D nano-materials, the electrospinning method is more versatile and convenient than the other processes for synthesizing organic and inorganic nanofibers [1,18-19]. The nanofibers have many industrial applications used

in a variety of fields such as sensors, filtration, biological cells, electronic devices, and protective clothing, etc [19-20].

Among the 1D transition metal oxides, ZnO has some distinct characteristics such as being non-toxic, having a wide band gap of 3.37 eV at room temperature, having a largely excited binding energy, being inexpensive, and containing photochemical properties. Moreover the 1D nano-sized ZnO is suitable candidate for solar cells, sensors, and optoelectronics devices due to its transparent and conductive property [1,21-22].

Recently, ZnO nanofibers with high crystallinity have been successfully fabricated using the electrospinning process. Despite the unique properties of ZnO, research on the influence of the oxidation states of ZnO dependent on the calcined temperature is still lacking.

Therefore, we studied ZnO nanofibers calcined at different temperatures, which were characterized by scanning electron microscopy (SEM), X-ray diffraction (XRD), transmission electron microscopy (TEM), and X-ray photoelectron spectroscopy (XPS).

3.2. Experimental Section

To fabricate 1D nanostructure zinc oxide (ZnO) nanofibers, electrospinning process was adopted. Two separate solutions, one containing zinc acetate ($Zn(CH_3COO)_2 \cdot 2H_2O$, MW: 219.51, Junsei Chemical) and the other containing polyvinylpyrrolidone (PVP, $(C_6H_9NO)x$, MW:~1,300,000, Sigma Aldrich) were prepared for precursor. The PVP solution was made by dissolving 0.77 g of PVP into 13 ml of ethanol (EtOH, 99.9 %) and the other solution was made by having 3 g of zinc acetate being added into 10 ml of distilled water. Both solutions were stirred for 5 hrs at room temperature separately. After this step, 1.0 ml of the zinc acetate solution was transferred to the PVP-EtOH solution then the mixed solution was vigorously stirred for 5 hrs at rt. The Zn/PVP solution had a reading of 42.65 cP of viscosity measured with a viscometer (SU-10, A&D). The mixed solution was used as a precursor for electrospinning. The Zn/PVP solution was loaded to a plastic syringe (10 ml) equipped with a flat tip of 21-gauge stainless needle. The syringe was placed on a syringe pump (KDS scientific) which was adjusted to 16 μl/min of feeding rate. A high voltage of

10.3 kV was applied to the metal needle tip. And an electrically grounded drum collector was covered with aluminum foil and rotated at 100 revolutions per minute. The working distance between the drum collector and the needle tip was fixed at 15 cm during the electrospinning process. The electrospun Zn/PVP nanofibers were initially dried to evaporate the residual organic solvent in the nanofiber. During the drying process, the temperature was kept at 353K with a tube furnace (DTF-40300-12T, Daeheung Scientific Co.) for 5 hrs in ambient environment. Then the dried ZnO nanofibers (Zn-rt) were calcined at 873 and 1173K based on the previous research of thermo-gravimetric analysis [23]. Hereafter, the ZnO nanofibers calcined at 873 and 1173K are named as Zn-873 and Zn-1173, respectively. Surface morphologies of the ZnO nanofibers were investigated using FE-SEM (JEOL, JSM-6700F). And the phase and crystallinity of ZnO nanofibers were checked by XRD (PHILIPS, X'Pert-MPD System) and TEM (JEOL, JEM-2010). To characterize the chemical nature of the ZnO nanofibers, XPS (VG Escalab MK II) was performed. The XPS system was recently rebuilt and calibrated in our

laboratory.

3.3. Results and Discussion

3.3.1. SEM analysis

Figure 3.1 shows the SEM images of the morphologies of Zn-rt, Zn-873, and Zn-1173. As shown in Figure 3.1 (a), Zn-rt was uniform, smooth, and continuous nanofibers which have 149 (± 2) nm of average diameter. Figures 3.1 (b) and (c) show that post-calcined ZnO nanofibers of Zn-873 and Zn-1173 have average diameters of 57 (± 1) and 207 (± 6) nm, respectively. As the calcination temperature increased to 873K, the PVP in/on Zn-rt nanofibers decomposed and evaporated, so ZnO crystals emerged on the surface, which has a coarse surface and decreased diameter. After calcination at 1173K for 5 hrs, the ZnO nanofibers looked like interconnected balls with a rougher surface and a larger diameter than those of Zn-rt. This observation indicates that the PVP could maintain the scaffold of nanofibers and decomposed from Zn/PVP nanofibers by calcination. As the calcination temperature increased to 873K, the ZnO particles of the internal parts of Zn-rt nanofiber could be observed and the diameter decreased due to the decomposition of PVP in the nanofibers. After

reaching a higher calcination temperature, 1173K, the ZnO crystals may be aggregated together, consequently, the diameter of Zn-1173 increased more, comparing with that of Zn-873. Therefore, the diameter and morphology of the ZnO are strongly dependent on the calcination temperature.

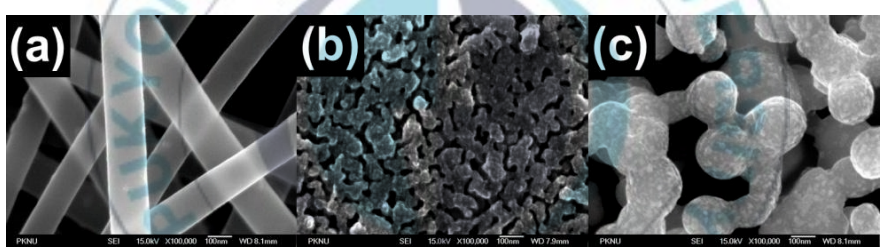

Figure 3.1. The SEM images of ZnO nanofibers of (a) Zn-rt, (b) Zn-873, and (c) Zn-1173. The size of scale bar in the figure is 100 nm.

3.3.2. XRD analysis

In order to investigate the crystalline phase and the function of the calcination temperature for the nanofibers, the XRD patterns of Zn-rt, Zn-873, and Zn-1173 were taken and shown in Figure 3.2. The diffraction pattern of Zn-rt shows no characteristic diffraction. This implies that the Zn-rt nanofibers have amorphous and polymeric properties. As the calcination temperature increased to 873 and 1173K, all apparent diffraction peaks confirmed the formation of the pure hexagonal close packed (hcp) ZnO phase with high crystallinity [24]. The observed XRD patterns of Zn-1173 have sharper and stronger peak intensity than those of Zn-873. The average crystallite size of ZnO nanofibers was deduced with (101) peak at $2\theta = 36.25^{o}$ using the well known Debye-Scherrer's equation [25]. The calculated average crystal sizes of Zn-873 and Zn-1173 are 24.98 (± 1.13) and 43.69 (± 1.73) nm, respectively. These observations suggest that the calcination process can play a role to remove the PVP from Zn-rt nanofibers and improve the crystallinity of ZnO nanofibers. Moreover, as the calcination temperature increased from 873 to 1173K, the crystal

sizes in calcined nanofibers become larger due to the aggregation of each nanoparticle in ZnO nanofibers. These results are in agreement with SEM observation.

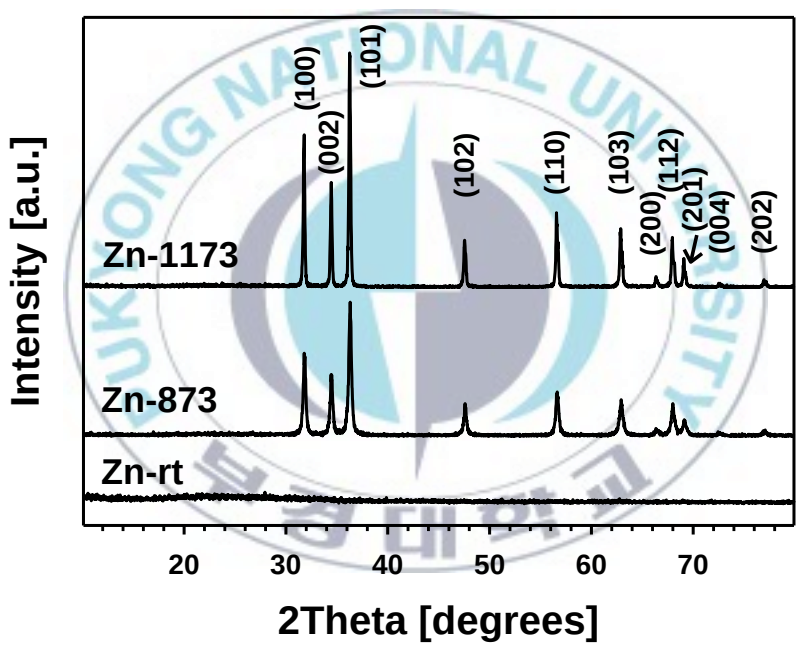

Figure 3.2. The XRD patterns of the Zn/PVP nanofibers (Zn-rt) and ZnO nanofibers calcined at different temperatures (Zn-873 and Zn-1173).

3.3.3. TEM analysis

For further investigation of the effect of calcination temperature on the ZnO nanofibers, TEM images of Zn-1173 were collected as shown in Figure 3.3. The Figures 3.3 (a) and (b) show high resolution TEM images taken at different sites of Zn-1173 nanofibers which show parallel arrangement revealing the crystallinity of ZnO nanofibers. The regular lattice fringes of Figure 3.3 (a) and (b) were approximately 0.28 (± 0.07) and 0.26 (± 0.08) nm, respectively. Those values correspond to the hcp ZnO of (100) and (002) plane, respectively. The Figures 3.3 (c) and (d) show the selected area electron diffraction (SAED) patterns indexing [001] and [010] directions of the hexagonal wurtzite ZnO structure. SAED results were also confirmed the crystalline structure of the ZnO nanofibers calcined at 1173K [26]. This observation clearly matched with the d-spacing of the XRD results of the ZnO [24]. It could explain that the crystallinity of the ZnO nanofibers is developed by the calcination process.

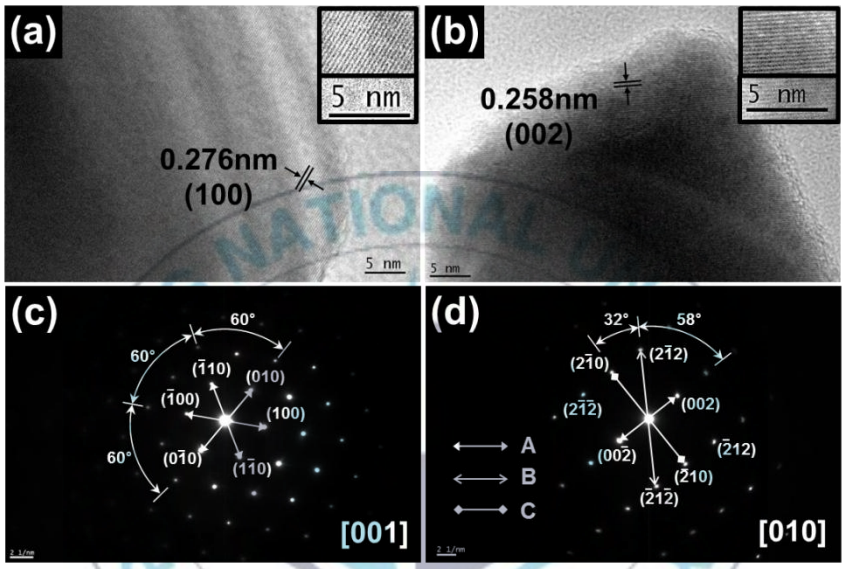

Figure.3.3. The high resolution TEM images in (a) and (b) and the selected area electron diffraction (SAED) patterns in (c) and (d) of Zn-1173 nanofibers.

3.3.4. XPS analysis

The chemical environment of the ZnO nanofibers was examined with XPS. As the calcination temperature increased Zn 2p peaks were pronounced and the characteristic peak of PVP, N 1s peak, was diminished shown in Figure 3.4. The C 1s peak was decreased by calcination at high temperatures as well. Even though the calcination system was evacuated during calcination, the decomposed carbon species from PVP was partially re-deposited on the surface region of the ZnO nanofibers. This might be the cause of the existence of carbon species on the nanofibers.

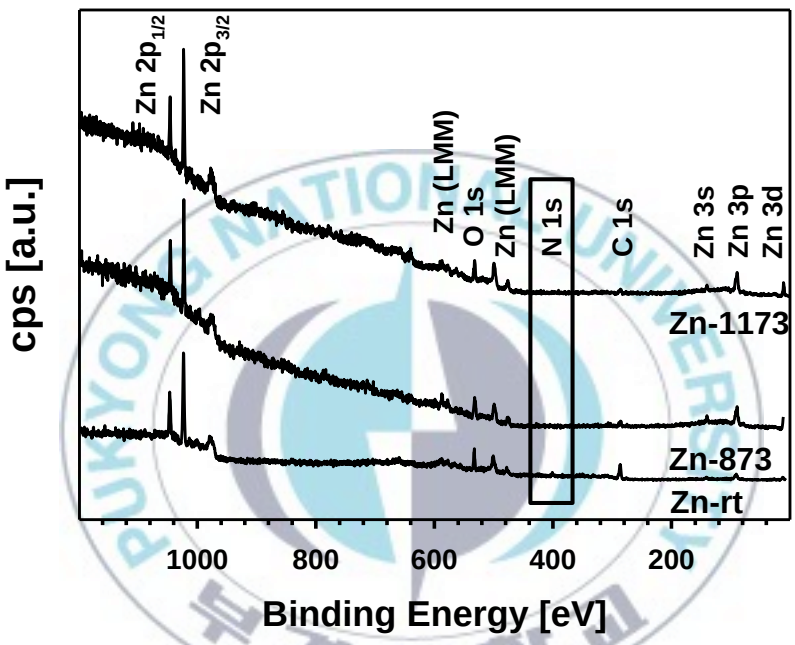

Figure 3.4. XPS Survey spectra of ZnO nanofibers of Zn-rt, Zn-873, and Zn-1173.

The detailed binding energies of carbon species were assigned after the deconvolution process with high-resolution XPS spectra of C 1s binding energy region. All XPS spectra shown here were referenced with adventitious carbon at 284.6 eV [28]. The chemical structure of PVP was shown in the inset of Figure 3.5. The labels shown in the chemical structure assigned from low to high binding energy side depending on the chemical environment of the carbon. The four deconvoluted C 1s peaks were assigned to the carbons as C-C (denoted C1, 284.6 ± 0.1 eV), C-C=O (C2, 285.6 ± 0.1 eV), C-N (C3, 286.4 ± 0.1 eV), and C=O (C4, 288.4 ± 0.1 eV). The atomic ratio of C1:C2:C3:C4 of Zn-rt was 2.04:1.00:2.35:1.24 which is close to the ratio of carbon species in PVP. As calcination temperature increased, the total intensity of carbon species decreased and the ratio among carbon species with different oxidation states changed. The peak intensities of C1, C3, and C4 drastically decreased due to the decomposition of PVP from the ZnO nanofibers. However, the C2 intensity did not change much. The re-deposited carbon species on the ZnO

nanofiber might exist as a carbonyl species. This observation is quite consistent with the O1s XPS results shown in Figure 3.6 (a).

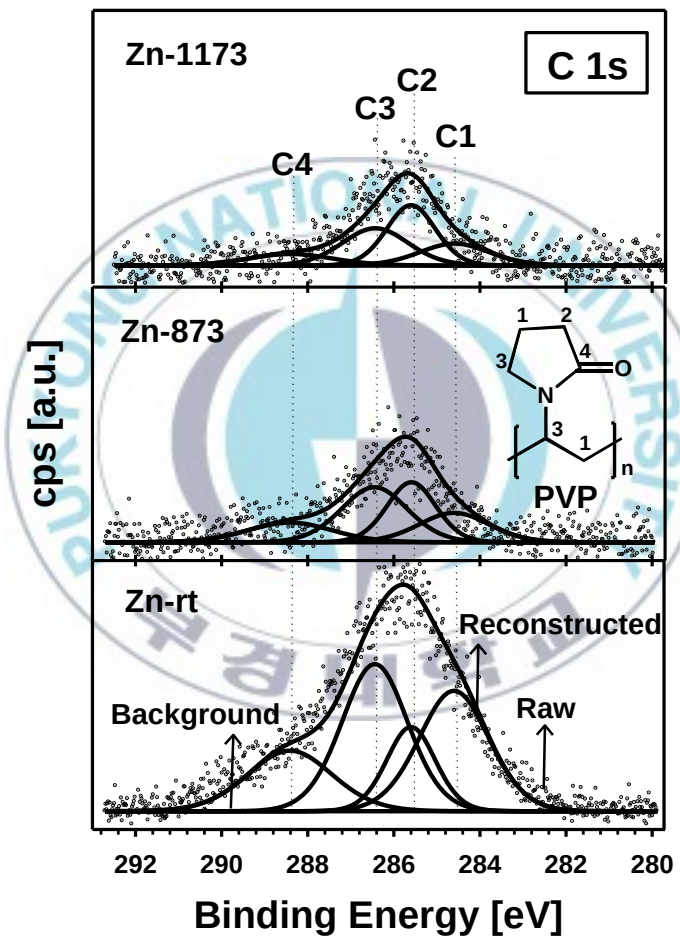

Figure 3.5. The deconvoluted high resolution the C 1s XPS spectra of Zn-rt, Zn-873, and Zn-1173. (inset is molecular structure PVP).

The deconvoluted high resolution O 1s and Zn $2p_{3/2}$ XPS spectra are shown in Figures 3.6 (a) and (b), respectively. Due to the large spin-orbit coupling constant of Zn 2p (23.1 eV), Zn $2p_{3/2}$ peak was deconvoluted and shown in the figure for clarity. Three oxidation states for oxygen and two oxidation states for zinc were assigned after peak deconvolution. The assigned binding energies of O 1s are Zn-O (530.5 ± 0.1 eV), Zn-(OH) (531.7 ± 0.1 eV), and Surf-O/CO (533.1 ± 0.1 eV). The assigned binding energies of Zn $2p_{3/2}$ are centered at 1021.5 ± 0.1 [29] and 1022.7 ± 0.1 eV for Zn^0 and Zn^{2+}, respectively. The assigned binding energies of O 1s and Zn $2p_{3/2}$ are in agreement with the previously reported values [30, 31].

As shown in Figure 3.6, thermal oxidation of zinc was observed by calcination of ZnO nanofibers. The atomic contents of Zn^0 and Zn^{2+} in Zn-rt were 47.3 and 52.7 at.%. After calcination of ZnO nanofibers at 1173K, the atomic contents of Zn^0 and Zn^{2+} changed to 88.1 and 11.9 at.%, respectively. The thermal oxidation of Zn was easily established by calcination [32]. The contents of Surf-O/CO were almost constant as 20.2, 18.9, and 15.7 at.% for

Zn-rt, Zn-873, and Zn-1173, respectively. These phenomena could indirectly explain the existence of re-deposited carbonyl species on the ZnO nanofibers after calcination. However, the ratio of $Zn(OH)_2$ to ZnO in Zn-rt, and Zn-1173 (Figure 3.6 (a)) were converted from 47.7:32.1 to 29.7:54.6. This might have happened because the hydroxide species could have decomposed and evaporated as H_2O during the calcination process. The total amount of oxygen bound with Zn^{2+} (ZnO and $Zn(OH)_2$) were 79.8, 81.1, and 84.3 at.% in Zn-rt, Zn-873, and Zn-1173, respectively. The increased amounts of oxygen and Zn^{2+} from Zn-rt to Zn-1173 are 4.5 and 35.4 at.%, respectively. After careful consideration of atomic sensitivity factors of O 1s (0.63) and Zn 2p (5.3) [28], the deduced chemical formula was $Zn_{6.68}O_{7.14}$ which is close to the stoichiometric compound, ZnO.

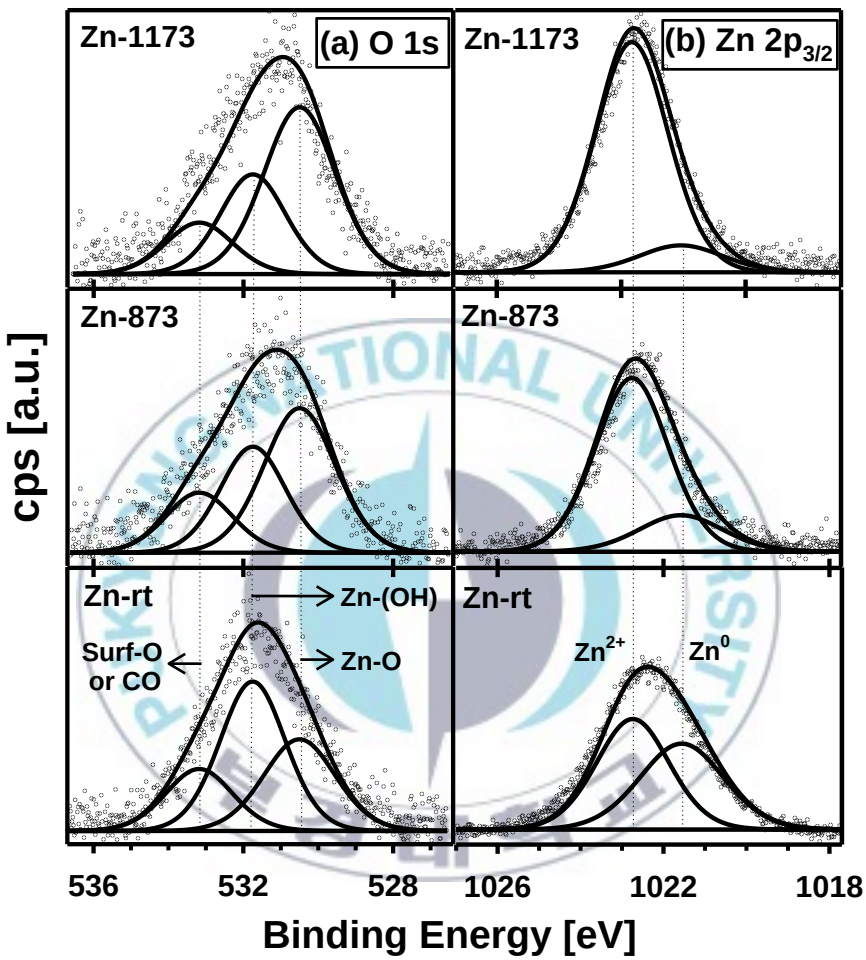

Figure 3.6. Representative XPS spectra of (a) O 1s and (b) Zn $2p_{3/2}$ of as electospun nanofibers and ZnO nanofibers calcined at 873 and 1173K.

3.4. Conclusion

In conclusion, the diameter of calcined ZnO nanofibers increased as the calcination temperature increased. And the total intensity of the carbon species decreased due to the decomposition of PVP in the nanofiber as the calcination temperature increased. In addition, as the effects of calcination temperature on the oxidation states of ZnO is still not well documented in other literatures, we used the XPS to characterize and identify the thermal oxidation of Zn species in the ZnO nanofibers. The initial ZnO nanofibers contained the two oxidation states, Zn^0 and Zn^{2+} in almost equal amounts. However, as the calcination temperature increased, the amount of Zn^{2+} amply increased while Zn^0 decreased. This means that the calcination promoted the oxidation of Zn species.

3.5. References

[1] Liu, L.; Li, S.; Zhuang, J.; Wang, L.; Zhang, J.; Li, H.; Li, Z.; Han, Y.; Jiang, X.; Zhang, P. *Sen. Act. B* **2011**, *155*, 782.

[2] Yiquan, W.; Zexuan, D.; Nathan, J.J.; Robert, L.C. *Mater. Lett.* **2011**, *65*, 2683.

[3] Yang, M.; Xie, T.; Peng, L.; Zhao, Y.; Wang, D. *Appl. Phys. A* **2007**, *89*, 427.

[4] Song, J.H.; Wang, X.D.; Liu, J.; Liu, H.B.; Li, Y.L.; Wang, Z.L. *Nano Lett.* **2008**, *8*, 203.

[5] Park, D.; Tak, Y.; Kim, J.; Yong, K. *Surf. Rev. Lett.* **2007**, *14*, 1061.

[6] Sun, Z.P.; Liu, L.; Zhang, D.Z. *Nanotechnology* **2006**, *17*, 2266.

[7] Bagci, V. M. K.; Gulseren, O.; Yildirim, T.; Gedik, Z.; Ciraci, S. *Phys. Rev. B* **2002**, *66*, 045409.

[8] Liao, L.; Lu, H.B.; Li, J.C.; Liu, C.; Fu, D.J.; Liu, Y.L. *Appl. Phys. Lett.* **2007**, *91*, 173110.

[9] Xu, W.Z.; Ye, Z.Z.; Ma, D.W.; Lu, H.M.; Zhu, L.P.; Zhao, B.H.; Yang, X.D.; Xu, Z.Y. *Appl. Phys. Lett.* **2005**, *87*, 093110.

[10] Qi, Q.; Zhang, T.; Wang, S.; Zheng, X. *Sens. Act. B Chem*. **2009**, *137*, 649.

[11] Spinolo, G.; Ardizzone, S.; Trasatti, S. *J. Electroanal. Chem.* **1997**, *423*, 49.

[12] Jung, B. O.; Kim, D. C.; Kong, B. H.; Lee, J. H.; Lee, J. Y.; Cho, H. K. *Eletrochem. Sol. St. Lett.* **2011**, *14*, H446.

[13] Noguchi, S.; Mizuhashi, M. *Thin Solid Films* **1981**, *77*, 99.

[14] Liu, Y.; Mi, C.; Su, L.; Zhang, X. *Electrochim. Acta*. **2008**, *53*, 2507.

[15] Dan, L.; Younan, X. *Adv. Mater*. **2004**, *16*, 1151.

[16] Ramaseshan, R.; Sundarrajan, S.; Jose, R.; Ramakrishna, S. *J. Appl. Phys*. **2007**, *102*, 111101.

[17] Hu, C.C.; Cheng, C.Y. *Electrochem. Solid-State Lett.* **2002**, *5*, A43.

[18] Ding, B.; Ogawa, G.; Kim, J.; Fujimoto, K.; Shiratori, S. *Thin Solid Films* **2008**, *516*, 2495.

[19] Park, J.A.; Moon, J.; Lee, S.J.; Lim, S.C.; Zyung, T. *Curr. Appl. Phys*. **2009**, *9*, S210.

[20] Venugopal, J.; Ramakrishina, S. *Appl. Biochem. Biotech*. **2005**, *125*, 147.

[21] Wu, Y.; Dong, Z.; Jenness, N.J.; Clark, R.L. *Mater. Lett.* **2011**, *65*, 2683.

[22] Sangkhaprom, N.; Supaphol, P.; Pavarajarn, V. *Ceram. Intern*. **2010**, *36*, 357.

[23] Jo, J.M.; Park, J.Y.; Kim, D.; Koh, S.W.; *Kang*, Y.C. *Bull. Korean Chem. Soc.* **2010**, *31*, 1776.

[24] JCPDS Database, International Center for Diffraction Data **1997**, PDF 80-0075.

[25] Klong, H.P.; Alexander, L.E. *X-ray Diffraction Procedures for Crystalline and Amorphous Materials, Wiley*: New York, **1954**; pp 491-538.

[26] Wang, Y.; Zhong, Z.; Chen, Y.; Ng, C.T.; Lin, J. *Nano Res*. **2011**, *4*, 695.

[27] Espitia-Cabrera, I.; Orozco-Hernandez, H. D.; Bartolo-Perez, P.; Contreras-Garcia, M.E.; *Surf. Coat. Technol.* **2008**, *203*, 211.

[28] Wagner, C. D.; Riggs, W. M.; Davis, L. E.; Moulder, J. F.; Muilenberg, G. E. *Handbook of X-ray Photoelectron Spectroscopy,*

Perkin-Elmer Corp.: USA. **1979**.

[29] Islam, M.N.; Ghosh, T.B.; Chopra, K.L.; Acharya, H.N. *Thin solid Films* **1996**, *280*, 20.

[30] Sepulveda-Guzman, S.; Reeja-Jayan, B.; Rosa, E.; Torres-Castro, A.; Gonzalez-Gonzalez, V.; Jose-Yacaman, M. *Mater. Chem. Phys*. **2009**, *115*, 172.

[31] Shiva, H.; Nilima, H.; David, L.; Bruce, C. *Nanoscale. Res. Lett.* **2009**, *4*, 1421.

[32] Guo, C.F.; Wang, Y.; Liu, Q. *J. Nanosci. Nanotechno*. **2010**, *10*, 1.

KOREAN ABSTRACT

나노 구조의 크기의 물질들은 흥미로운 특성과 양상으로 인해 연구주제로 널리 사용 되어왔다. 이 논문에는 전기방사법에 의한 Co 와 Zn 산화물 마이크로, 나노섬유의 제조와 그 특성들에 대하여 연구 하였다.

코발트 산화물 마이크로섬유를 전기방사법을 이용해서 합성하였고, 높은 온도에서 열처리 이후에 Co_3O_4 마이크로섬유가 형성되었다. 이 열처리 온도는 섬유의 직경, 형태, 결정 상, 그리고 화학적 환경에 영향을 미친다. 전계주사현미경 (SEM)을 이용해서 얻어진 섬유의 표면형태를 관측할 수 있었다. 상온에서부터 873, 1173K 으로 열처리 온도가 증가함에 따라서 각 온도에서 산화코발트 섬유의 직경이 1.79, 0.82, 0.32 μm 로 감소됨이 측정되었다. 섬유의 구조에 관한 연구는 X-선 회절분석(XRD)와 투과전자현미경 (TEM)을 이용해 조사하였고 열처리된 Co_3O_4 섬유가 면심입방결정 (fcc)을 가지는 것을 확인할 수 있었다. X-선 광전자 분광법 (XPS) 결과는 증가된 열처리 온도는 Co^{2+}와 Co^{3+}의 형성을 증진시키는 것으로 나타났다.

수 많은 금속 산화물 중 Zn oxide 을 선택하여 전기방사법을 통해 나노섬유를 합성하였다. 이것은 태양전지와 센서로 사용될 수 있는 가능성이 있다. ZnO 나노섬유가 얻어진 이후에 열처리 온도가

나노섬유에 영향을 준다는 사실이 연구 되었다. SEM 의 결과로 ZnO 나노섬유가 응집이 열처리로 인해서 진행 되었다는 것이 드러났다. XRD 연구로 873, 1173K 에서의 열처리로 hcp ZnO 구조가 성장하는 것을 확인할 수 있었다. TEM 실험으로 열처리 된 ZnO 나노섬유의 결정성을 확인 할 수 있었다. XPS 는 나노섬유내의 Zn 화학종이 열처리로 인해 thermal oxidation 됨을 확인할 수 있었다. 이러한 연구를 통해 열처리 온도가 증가 될수록 ZnO 의 직경의 증가 되는 것과 열처리 과정이 ZnO 나노섬유의 결정성에 영향을 주는 것과 Zn 화학종의 thermal oxidation 이 열처리 온도가 증가될수록 진행이 된다는 사실을 도출할 수 있었다.

ACKNOWLEDGMENTS

이 논문이 나오기까지 수많은 분들의 도움과 격려가 있었습니다. 이 페이지를 빌어 감사를 표현해보려 합니다.

먼저, 제 지도교수님이신 강용철 교수님, 정말 감사 드립니다. 수많은 과정과 실패 속에서 좋은 결과를 낼 수 있다는 것을 많은 기기를 고치시는 모습을 보면서, 논문을 함께 쓰면서, 부지런하고 실천하는 삶을 사시면서 몸소 가르쳐 주셔서 감사합니다. 끝이라 생각하지 않고 교수님께서 보여주신 것처럼 그러한 삶을 살아가겠습니다. 그리고 늘 조언을 아끼지 않으시고 기꺼이 심사를 해주신 김주창 교수님, 김돈 교수님께도 정말 감사 드립니다. 또한 격려와 관심을 가지고 도와주신 화학과 교수님들께 감사드립니다.

SMIL 실험실 생활 2 년동안 함께 지내며 가르쳐주신 박주연 선배에게도 정말 감사 드립니다. 늘 이해해주고 격려해주고 조언을 늘 주셔서 감사드립니다. 그리고 졸업하였지만 함께 하였던 빈준형 선배, 황아름에게도 감사합니다. 아울러 대학원 동기들, 선배님, 후배들 모두 고맙습니다.

저의 가장 친한 친구들 대학원 생활 동안 서로 함께할 수 있었던 수경이, 멀리 있지만 격려를 아끼지 않은 인경이, 한솔, 화경, 신탁이, 걸, 용민, 지환, 명진 너무 고마워요. 그리고 감전교회 식구들 목사님, 길우, 유진, 혜빈, 유미, 수겸, 정헌, 상민, 은희, 혜련, 원민, 영재, 성희, 기영 바쁜 저를 이해해주고 늘 함께 해주셔서 고맙습니다.

마지막으로 사랑하는 나의 가족과 할머니, 진심으로 깊은 감사의 마음 전해 드립니다. 사랑합니다. Thanks, God.


PUKYONG NATIONAL UNIVERSITY
부경대학교